QUASAR CLUSTERING AND SPACETIME GEOMETRY

Piotr A. Popowski, David H. Weinberg, Barbara S. Ryden, and Patrick S. Osmer

Ohio State University, Dept. of Astronomy, Columbus, OH 43210

E-mail: popowski, dhw, ryden, posmer @astronomy.ohio-state.edu

Received _____; accepted _____

arXiv:astro-ph/9707175v1 15 Jul 1997

ABSTRACT

The non-Euclidean geometry of spacetime induces an anisotropy in the apparent correlation function of high-redshift objects, such as quasars, if redshifts and angles are converted to distances in "naive" Euclidean fashion. The degree of angular distortion depends on cosmological parameters, especially on the cosmological constant Λ, so this effect can constrain Λ independent of any assumptions about the evolution of luminosities, sizes, or clustering. We examine the prospects for distinguishing between low-density ($\Omega_0 = 0.1 - 0.4$) cosmological models with flat and open space geometry using the large quasar samples anticipated from the Two Degree Field Survey (2dF) and the Sloan Digital Sky Survey (SDSS). Along the way, we derive a number of results that are useful for studies of the quasar correlation function. In particular, we show that even these large quasar surveys are likely to reside in the "sparse sampling" regime for correlation function measurements, so that the statistical fluctuations in measurements are simply the Poisson fluctuations in the observed numbers of pairs. As a result: (a) one can devise a simple maximum-likelihood scheme for estimating clustering parameters, (b) one can generate Monte Carlo realizations of correlation function measurements without specifying high-order correlation functions or creating artificial quasar distributions, and (c) for a fixed number of quasars, a deeper survey over a smaller area has greater statistical power than a shallow, large-area survey. If the quasar correlation length is equal to the value implied by recent (quite uncertain) estimates, then the 2dF and SDSS samples can provide clear discrimination between flat and open geometries for $\Omega_0 \leq 0.2$ but only marginal discrimination for $\Omega_0 = 0.4$. Clear discrimination is possible for $\Omega_0 = 0.4$ if the true quasar correlation length is a factor of two larger, and a high-density survey of 30,000 quasars in 200 square degrees would provide

clear discrimination even for the lower correlation length. Detection of quasar clustering anisotropy would confirm the cosmological spacetime curvature that is a fundamental prediction of general relativity.

Subject headings: quasars: general, large-scale structure of Universe

1. Introduction

In cosmological models that obey General Relativity and the cosmological principle, the mass density parameter, Ω, and the cosmological constant, Λ, together determine the geometry of spacetime. The Einstein-de Sitter ($\Omega = 1$) model has twin virtues of simplicity: flat spatial geometry and zero cosmological constant. However, the ages of globular cluster stars, the high baryon fraction in galaxy clusters, and some aspects of large scale galaxy clustering are accounted for more easily in low density models, which have flat geometry if $\lambda_0 \equiv \Lambda c^2/3H_0^2 = 1 - \Omega_0$ [1], or open, negative curvature geometry if $\Lambda = 0$. Dynamical studies of large scale structure can constrain Ω_0 (subject to uncertainties about biased galaxy formation), but they are insensitive to a cosmological constant because it represents an unclustered energy component. This paper examines the prospects for using the anisotropy of the quasar correlation function to constrain Ω_0 and λ_0, in particular to distinguish between flat and open cosmologies. While this test is impractical with present quasar samples, the Anglo-Australian 2-degree Field Survey (hereafter 2dF) and the Sloan Digital Sky Survey (hereafter SDSS or Sloan) will both produce redshift samples of several tens of thousands of quasars over the next few years.

Classical methods of measuring spacetime geometry rely on standard candles or standard rulers, and they are therefore subject to systematic uncertainties in the evolution of these objects over a large range in redshift. Alcock & Paczyński (1979) proposed an alternative approach that is almost entirely independent of evolution and assumes only that structure in the universe is statistically isotropic, as implied by the cosmological principle. At high redshift, the ratio of distances corresponding to a given redshift separation Δz and angular separation $\Delta\theta$ depends on the spacetime metric, and one can constrain the

[1]Subscript 'zero' indicates the value of the parameters at the present epoch. Also, we use the notation $H_0 \equiv \mathrm{h}_0 \cdot 100$ km s^{-1} Mpc^{-1}

cosmological parameters by requiring that they yield isotropic structure.

Alcock & Paczyński (1979) illustrated their suggestion with the idealized example of spherical clusters, but nature does not provide us with such convenient objects of study. Ryden (1995a) suggested using the statistical distribution of void shapes in deep galaxy redshift surveys like the SDSS, but it is not clear that even this million galaxy sample will be sufficient to detect the effect; it does not extend much beyond $z \sim 0.2$, and at this depth the geometrical distortion of voids is difficult to separate from distortions induced by galaxy peculiar velocities (Ryden & Melott 1996). While quasar redshift surveys have fewer tracers, they reach to much higher redshifts, where the expected geometrical anisotropy is more pronounced. Thus Phillips (1994) suggested using the orientations of neighboring quasar pairs to implement Alcock & Paczyński's method. The 2-point correlation function contains statistical information on the distribution of all quasar pairs, not just nearest neighbor pairs, so it is a more powerful measure for detecting distortions of geometry. It is important to note that these distortions are detectable only because quasars are clustered. If quasars were Poisson distributed, then all pair orientations would be statistically isotropic regardless of the assumed metric.

Two recent papers (Ballinger, Peacock & Heavens 1996; Matsubara & Suto 1996; see also Nakamura, Matsubara, & Suto 1997) have discussed the use of redshift space clustering in quasar samples as a tool for constraining Ω_0 and λ_0. Matsubara & Suto (1996) derive an expression for the correlation function that includes the effects of geometrical distortion and linear theory peculiar velocities. Ballinger et al. (1996) derive expressions for the redshift space power spectrum, including effects of geometrical distortion, linear theory peculiar velocities, and incoherent random velocities generated by small scale collapse.

In the next section, we discuss the geometrical distortion of the correlation function in the absence of peculiar velocities, extending the calculation of Phillips (1994). The

distortion due to geometry alone is simple to understand: changes in the metric just alter the relation between a $(\Delta z, \Delta\theta)$ separation and the corresponding physical distance. In §3 we show that, for realistic quasar samples, measurement errors in the correlation function are likely to be dominated by Poisson fluctuations in the number of quasar pairs. As a result, we can easily create Monte Carlo realizations of correlation function measurements for a specified model correlation function. In §4 we use such Monte Carlo experiments to see what cosmological constraints can be expected from the 2dF and Sloan quasar samples. In §5 we summarize the results of these experiments and discuss some of their limitations. The most serious of these is probably our neglect of peculiar velocity distortions in modeling the correlation function, but we argue in §5 that these are unlikely to overwhelm the geometrical signal. A full analysis of observational data will require joint consideration of velocity and geometry effects, along the lines envisioned by Ballinger et al. (1996).

2. The redshift space correlation function

The position of a quasar in redshift survey data is characterized by three numbers: the redshift and two angle coordinates on the sky (z, θ_r, ϕ_r). For a given quasar, the probability of finding a neighbor in a given volume element is symmetric about the line of sight, since this is the only preferred direction. For any pair of quasars one can therefore find a transformation $(\phi_r, \theta_r) \rightarrow (\phi, \theta)$ such that $\phi_1 = \phi_2$ in the new frame of reference. Consequently, the distance between the points in redshift space can be described in terms of redshift z and angle θ.

Figure 1 shows the situation with quasars at the positions (z_1, θ_1) and (z_2, θ_2). We define $s_z \equiv z_2 - z_1$, $s_\theta \equiv z \cdot (\theta_2 - \theta_1) = z \cdot \Delta\theta$, with $z = (z_1 + z_2)/2$ assumed to be much

greater then $z_2 - z_1$. We now adopt the following notation:

$$s \equiv \sqrt{s_z^2 + s_\theta^2}\,, \tag{1}$$

and

$$\mu \equiv \frac{s_z}{s}\,. \tag{2}$$

The angular separation can then be expressed as

$$\Delta\theta^2 = z^{-2} s_z^2 (\mu^{-2} - 1). \tag{3}$$

In Euclidean geometry, s_z and s_θ would be the line-of-sight and transverse separations, respectively (in dimensionless, redshift units); s would be the 3-dimensional separation, and μ would be the cosine of the angle between the separation vector and the line of sight. In reality the geometry is not Euclidean, but we can still keep the formal definitions of s and μ introduced above.

Adopting Phillipps' (1994) notation we have

$$r^2 = f^2 \Delta\theta^2 + g^2 s_z^2\,, \tag{4}$$

where in general (e.g., Weinberg 1972)

$$f = \frac{c}{H_0} \times \begin{cases} \frac{1}{\sqrt{1-\Omega_0\ -\lambda_0}} \sinh\left[\int_{\frac{1}{1+z}}^{1} \frac{\sqrt{1-\Omega_0\ -\lambda_0}dy}{y\sqrt{\frac{\Omega_0}{y} - (1-\Omega_0\ -\lambda_0) + \lambda_0 y^2}}\right] & \text{if } (\Omega_0\ +\lambda_0) < 1 \\ \int_{\frac{1}{1+z}}^{1} \frac{dy}{y\sqrt{\frac{\Omega_0}{y} + \lambda_0 y^2}} & \text{if } (\Omega_0\ +\lambda_0) = 1 \\ \frac{1}{\sqrt{-(1-\Omega_0\ -\lambda_0)}} \sin\left[\int_{\frac{1}{1+z}}^{1} \frac{\sqrt{-(1-\Omega_0\ -\lambda_0)}dy}{y\sqrt{\frac{\Omega_0}{y} - (1-\Omega_0\ -\lambda_0) + \lambda_0 y^2}}\right] & \text{if } (\Omega_0\ +\lambda_0) > 1 \end{cases} \tag{5}$$

and

$$g = \frac{c}{H_0} \times \frac{1}{\sqrt{\Omega_0\ (1+z)^3 + (1-\Omega_0\ -\lambda_0)(1+z)^2 + \lambda_0}}. \tag{6}$$

Combining equations (1), (2), (3) and (4), we find

$$\frac{r}{s} = g\sqrt{\mu^2 + h^2(1-\mu^2)}\ , \quad \text{where}\ \ h \equiv \frac{1}{z} \cdot \frac{f}{g}. \tag{7}$$

Now suppose that the quasars are clustered and that their correlation function $\xi(r)$ is described by power-law,

$$\xi(r) = \left(\frac{r}{r_0}\right)^{-\gamma}, \tag{8}$$

where, in principle, the correlation length r_0 and the index γ may be functions of z. In redshift space, the correlation function at vector separation (s, μ) is simply the value of $\xi(r)$ at the scalar separation r corresponding to s, μ. Substitution of (7) into (8) yields

$$\xi(s,\mu) = \left(\frac{s}{s_0}\right)^{-\gamma} \left[\mu^2 + h^2(1-\mu^2)\right]^{-\frac{\gamma}{2}}, \tag{9}$$

where $s_0 = r_0/g$. The correlation function in these coordinates is anisotropic because the physical separation corresponding to a given s depends on angle with respect to the line of sight. The anisotropy is stronger when γ is larger because a given change in r then produces a larger change in $\xi(r)$.

Once s_0 and γ are set, the dependence of the correlation function on the geometry of the universe is determined entirely through the value of the "distortion parameter" h. Figure 2 shows the redshift dependence of $h(z)$ for open and flat cosmologies with various Ω_0 . The functional form of $h(z)$ depends much more strongly on λ_0 than on Ω_0 , implying that clustering anisotropy can much more easily distinguish models with the same Ω_0 and

different λ_0 than models with similar λ_0 and different Ω_0, as Alcock & Paczyński (1979) pointed out. There is also an approximate degeneracy in $h(z)$ between open models with low Ω_0 and flat models with relatively high Ω_0.

In the range $1 < z < 5$, $h(z)$ can be well approximated by a straight line for most models. The anisotropy increases with redshift in all cases, but models can in principle be distinguished both by the value of h at a given z and by the overall redshift dependence of $h(z)$. As discussed in the following sections, in a real redshift survey the information for distinguishing cosmologies comes mainly from the redshifts where the quasar distribution peaks, since that is where the clustering can be measured most precisely.

Figure 3 shows the angular dependence of the correlation function, from equation (9), for various values of h. If $h = 1$, the geometry of redshift space is Euclidean, and there is no correlation function anisotropy. All models have $h \approx 1$ at $z \ll 1$, and the $\lambda_0 = 1$, $\Omega_0 = 0$ model has $h(z) = 1$ at all redshifts. For other models $h(z) > 1$ at high redshifts, and the correlation function is amplified[2] for pair separations along the line of sight ($|\mu| = 1$) relative to pair separations perpendicular to the line of sight. The anisotropy of the correlation function increases rapidly with increasing h.

[2]Whether one sees "amplification" or "suppression" depends on the choice of reference model. Here our reference is Euclidean (λ_0=1), but Ballinger et al. (1996) take Ω_0 =1 as a reference and therefore find that alternative models have suppressed clustering along the line of sight.

3. Statistical errors in measurements of $\xi(s,\mu)$

Following Peebles (1980, §31), we can define a quasar's average number of "clustered neighbors" by

$$N_c = \int_0^\infty \bar{n}\xi(r)4\pi r^2 dr, \tag{10}$$

where $\bar{n}$ is the space density of quasars in a sample. For purposes of calculation, we assume a power-law correlation function (equation [8]). Since the correlation function may fall below this power-law at large distances, we only consider pairs out to a separation αr_0 that is a small multiple α of the correlation length. Substitution of (8) into (10) yields

$$N_c = \frac{4\pi\alpha^{3-\gamma}}{3-\gamma}\bar{n}r_0^3. \tag{11}$$

We will take $\alpha = 2$ as a template value in our simulations. For $\alpha = 2$, the value of N_c from (11) varies by only 5% for $1 \le \gamma \le 2$.

Consider a sample of N_Q quasars in an area A square degrees, and let $F(z)dz$ denote the fraction of the quasar sample in the redshift range $(z, z+dz)$, normalized so that $\int_0^\infty F(z)dz = 1$. The observations directly tell us $(N_Q/A)F(z)$, the average number of quasars per square degree per unit redshift. The relation between $(N_Q/A)F(z)$ and the number density $\bar{n}(z)$ in comoving $\mathrm{h_0}^{-3}$ Mpc^3 depends on the cosmological model. Since the volume of a redshift range dz and solid angle $d\Omega$ is $g\,dz \cdot f^2 d\Omega$,

$$\bar{n} = \frac{3283(N_Q/A)F(z)}{gf^2}, \tag{12}$$

where 3283 is the number of square degrees per radian. For compactness, in this and future equations we generally omit the explicit z-dependence of $\bar{n}$, f, and g. From (5) and (6) it

is clear that both f and g involve the factor $cH_0^{-1} = 3000\mathrm{h_0}^{-1}$Mpc, and it is convenient to write them in the form

$$f = \frac{c}{H_0}\tilde{f}, \qquad \text{and} \qquad g = \frac{c}{H_0}\tilde{g}. \tag{13}$$

We use the notation (13) and the value of cH_0^{-1} to write (12) as

$$\bar{n} = 1.21 \cdot 10^{-7}\frac{N_Q}{A}F(z)\tilde{g}^{-1}\tilde{f}^{-2} \;\; \mathrm{h_0^3\ Mpc^{-3}\ (comoving)}. \tag{14}$$

Substitution of (14) into (11) gives

$$N_c(z) = \frac{4\pi\alpha^{3-\gamma}}{3-\gamma}r_0^3\left(1.21 \cdot 10^{-7}\frac{N_Q}{A}F(z)\tilde{g}^{-1}\tilde{f}^{-2}\right), \tag{15}$$

for r_0 in comoving $\mathrm{h_0^{-1}}$ Mpc. The number of correlated pairs in the range $(z, z+dz)$ is

$$N_{pairs}(z) = N_Q F(z) N_c(z) \propto \frac{N_Q^2}{A}F^2(z)r_0^3. \tag{16}$$

As a fiducial case let us take $\alpha = 2$, $\gamma = 2$, $N_Q = 10^5$, $A = 10^4\,\Box^\circ$, and $F(z) = 0.5$. Then

$$N_c(z) = 0.11\left(\frac{r_0}{10\mathrm{h_0}^{-1}\mathrm{Mpc}}\right)^3\left(\frac{\tilde{g}^{-1}\tilde{f}^{-2}}{7.27}\right), \tag{17}$$

where r_0 is the comoving correlation length. We have scaled $\tilde{g}^{-1}\tilde{f}^{-2}$ to the value for an Ω_0 =1 model at $z = 2$. Substitution of (17) into (16) yields

$$N_{pairs}(z) = 5500\left(\frac{r_0}{10\mathrm{h_0}^{-1}\mathrm{Mpc}}\right)^3\left(\frac{\tilde{g}^{-1}\tilde{f}^{-2}}{7.27}\right) \tag{18}$$

for the number of correlated quasar pairs expected in an interval $\Delta z \approx 1$ near the peak of the redshift distribution $F(z)$ in a large quasar redshift survey.

We now come to the central issue of this Section — a key issue for the entire paper, in fact — the nature of statistical fluctuations in estimates of the correlation function. In the limit $N_c \gg 1$, the statistical uncertainty is dominated by the finite number of independent structures in the survey volume, an effect sometimes referred to as "cosmic variance." As a conceptual toy model, one can imagine the structure to consist of clusters with an average of N_c members apiece. Each cluster is sampled by many correlated pairs, so the fluctuation in the number of clusters within the survey dominates the error in ξ. In the opposite limit, $N_c \ll 1$, most clusters are not "detected" with even a single correlated pair, and it is the Poisson fluctuation in the number of pairs that dominates the statistical error rather than the fluctuation in the number of independent structures. In this "sparse sampling" or "Poisson limit," the error in an estimate of $\xi(s, \mu)$ in a bin $(\Delta s, \Delta\mu)$ is simply the Poisson error in the number of pairs in the bin, and the errors in separate bins are statistically independent. The transition between the dense sampling and sparse sampling limits occurs at $N_c \approx 1$; we have carried out numerical experiments with Monte Carlo clustering models (Soneira & Peebles 1978) to confirm that the Poisson error approximation holds quite accurately for $N_c \lesssim 1$.

In a typical galaxy redshift survey, $N_c(z) \gg 1$ nearby, and $N_c(z)$ drops below one at large distances, where only the most luminous galaxies lie above the survey's apparent magnitude limit. Roughly speaking, the volume within which $N_c(z) \gtrsim 1$ is the effective volume of the survey for purposes of estimating ξ; there is some usable information from larger distances, but as the structure "fades out" under increasingly sparse sampling, the statistical significance of this additional information drops.

Equation (17) implies that even an ambitious quasar redshift survey is likely to be in the sparse sampling regime at *all* redshifts, unless the comoving quasar correlation length is substantially larger than $10 h_0^{-1}$ Mpc. This result has several important implications. First,

the independent, Poisson errors in ξ allow a straightforward maximum-likelihood scheme for estimating correlation function parameters. We describe this scheme in §4.3 below; this method was developed independently by Croft et al. (1997), who applied it to rich galaxy clusters, and it was applied to a sample of high-redshift quasars from the Palomar Transit Grism Survey by Stephens et al. (1997). A second implication is that, given a theoretical prediction of $\xi(s,\mu)$, one can generate Monte Carlo realizations of measured correlation functions for a given sample without creating detailed realizations of a clustering pattern, because the fluctuation in a measured value of ξ depends only on the expected number of pairs and is independent of fluctuations in other bins and of the higher-order clustering properties of the quasar distribution. We describe this method for creating Monte Carlo realizations in §4.2 below, and in §4.4 we use it to evaluate the power of the SDSS and 2dF quasar redshift surveys for constraining the cosmological constant. Finally, there is an observational implication: for a fixed number of quasars, a deeper survey over a smaller area has greater statistical power, at least for measurements of the correlation function on scales $\sim r_0$.

This last point is demonstrated most clearly by generalizing equations (17) and (18) to

$$N_c(z) = 0.11 \left(\frac{\alpha^{3-\gamma}/(3-\gamma)}{2}\right) \left(\frac{r_0(z)}{10h^{-1}\mathrm{Mpc}}\right)^3 \left(\frac{N_Q/A}{10/\Box^o}\right) \left(\frac{F(z)}{0.5}\right) \left(\frac{\tilde{g}^{-1}\tilde{f}^{-2}}{7.27}\right), \qquad (19)$$

$$N_{pairs}(z) = 5500 \left(\frac{\alpha^{3-\gamma}/(3-\gamma)}{2}\right) \left(\frac{r_0(z)}{10h^{-1}\mathrm{Mpc}}\right)^3 \left(\frac{N_Q}{10^5}\right) \left(\frac{N_Q/A}{10/\Box^o}\right) \left(\frac{F(z)}{0.5}\right)^2 \left(\frac{\tilde{g}^{-1}\tilde{f}^{-2}}{7.27}\right). \qquad (20)$$

If $N_c(z) \lesssim 1$, then the effective signal for correlation function measurements is set by $N_{pairs}(z)$, since each correlated pair contributes non-redundant information. At fixed surface density N_Q/A, this signal increases in proportion to the number of quasars N_Q, but at fixed area A it is proportional to N_Q^2. Of course, increasing N_Q at fixed A usually requires one to observe fainter quasars, while increasing N_Q at fixed surface density does

not. Equation (20) also implies that the precision of correlation function measurements will be peaked sharply near the maximum of the survey's redshift distribution $F(z)$ and that the precision attained will depend strongly on the actual value of the quasar correlation length r_0.

The remaining equations in this Section are not fundamental, but they are needed for our Monte Carlo simulations and maximum-likelihood parameter estimation, and we include their derivation for the convenience of others who may wish to pursue similar approaches. A physical model specifies the correlation function in real space (r-space), but a redshift survey provides data in redshift space (s-space). The relation between coordinates in these two complementary descriptions is

$$\begin{pmatrix} dr \\ d(\cos t) \end{pmatrix} = \underbrace{\begin{pmatrix} \frac{\partial r}{\partial s} & \frac{\partial r}{\partial \mu} \\ \frac{\partial(\cos t)}{\partial s} & \frac{\partial(\cos t)}{\partial \mu} \end{pmatrix}}_{\boldsymbol{A}} \begin{pmatrix} ds \\ d\mu \end{pmatrix}, \tag{21}$$

where $\cos t = g s_z / r$. Thus

$$dr\, d(\cos t) = \det \boldsymbol{A}\; ds\, d\mu. \tag{22}$$

A short calculation leads to

$$d(\cos t) = \frac{h^2 d\mu}{[h^2 - (h^2-1)\mu^2]^{\frac{3}{2}}}, \tag{23}$$

and

$$dr = g\sqrt{h^2 - (h^2-1)\mu^2}\, ds - \frac{gs\mu(h^2-1)d\mu}{\sqrt{h^2-(h^2-1)\mu^2}}. \tag{24}$$

Since $\frac{\partial(\cos t)}{\partial s} = 0$, equation (22) yields

$$(dV)_r = -2\pi r^2 dr d(\cos t) = -2\pi r^2 \left[\frac{\partial r}{\partial s} \cdot \frac{\partial(\cos t)}{\partial \mu}\right] ds d\mu \tag{25}$$

for the volume element in real space. Substitution of (23) & (24) into (25) leads to

$$(dV)_r = g^3 h^2 (-2\pi s^2 ds d\mu) = g^3 h^2 (dV)_s, \tag{26}$$

where $(dV)_s$ is the volume element in redshift space. The number of quasars in a given region will be the same regardless of the adopted coordinate system. Thus

$$n_s (dV)_s \equiv n(z)(dV)_r, \tag{27}$$

where n_s and $n(z)$ are number densities of quasars in redshift and real spaces, respectively. Combining (26) and (27) leads to

$$n_s(s,\mu) = g^3(z) h^2(z) n(z). \tag{28}$$

The number of pairs expected in an infinitesimally small bin in (s,μ) within the finite redshift range $(z, z+\Delta z)$ is

$$dN_{pairs} = N(z, z+\Delta z) n_s [1+\xi(s,\mu)](-2\pi s^2 ds d\mu), \tag{29}$$

where $N(z, z+\Delta z)$ is the number of observed quasars in this redshift range. Since $F(z)dz$ is the fraction of quasar redshifts in an infinitesimal range dz,

$$N(z, z+\Delta z) = N_Q \int_z^{z+\Delta z} F(z) dz, \tag{30}$$

where N_Q is the total number of quasars in the sample. Substitution of (9), (28) and (30) into (29) for infinitesimally small $\Delta z \equiv dz$ yields

$$dN_{pairs} = -2\pi N_Q g^3 h^2 \bar{n} F(z) \left\{ 1 + \left(\frac{s}{s_0} \right)^{-\gamma} \left[\mu^2 + h^2 (1-\mu^2) \right]^{-\frac{\gamma}{2}} \right\} s^2 dz ds d\mu. \tag{31}$$

Here $s_0 \equiv r_0/g$ is the line-of-sight separation that corresponds to the comoving correlation length r_0, and the mean number density $\bar{n}$ is given in terms of N_Q, A, and $F(z)$ by equation (14). The quantities g, h, and $\bar{n}$ all depend on redshift, and s_0 and γ may depend on redshift also.

4. Monte Carlo experiments

4.1. Observational perspective

Successful measurement of quasar clustering anisotropy will require redshift samples much larger than those that exist today. There are two clear prospects for such samples, the SDSS and a quasar redshift survey using the 2dF fiber spectrograph on the Anglo-Australian Telescope. The SDSS plans to obtain redshifts for 80,000 quasars in an area of 5,000 square degrees in the North Galactic Cap. It will also measure redshifts for $\sim 20,000$ quasars in the surrounding 5,000 square degree "skirt," but this subset will be less useful for clustering measurements because of its lower density. The SDSS will also conduct a deeper quasar survey in a stripe of ~ 200 square degrees in the South Galactic Cap, to a limiting magnitude yet to be determined. (A discussion of the planned SDSS quasar survey can be found at http://www.astro.princeton.edu/BBOOK/SCIENCE/QUASARS/quasars.html.) The SDSS will select quasar candidates based on 5-band CCD photometry. The planned 2dF survey will target $\sim 30,000$ quasars in an area ~ 750 square degrees, selected as UV-excess stellar objects on scanned photographic plates (Shanks, private communication).

In order to generate Monte Carlo realizations of correlation function measurements from these samples, we need to know (approximately) the expected redshift distributions $F(z)$. We have computed these using the observational determinations of the quasar luminosity function by Boyle (1991) and Warren, Hewett, & Osmer (1994). The Boyle

(1991) results are based on the Boyle, Shanks & Peterson (1988) survey of quasars selected by the UV-excess method, which is effective mainly for $z \lesssim 2.2$. The Warren et al. (1994) results are based on a multicolor survey and probe the redshift range $2.0 < z < 4.5$. For our calculations, we assume that the 2dF survey will contain quasars only up to $z = 2.2$, because of its UV-excess selection technique, and that the SDSS multi-color selection will identify quasars at all redshifts, with apparent magnitude being the only important limit. We find that the planned SDSS and 2dF surface densities imply limiting apparent magnitudes of roughly $B = 19.6$ and $B = 21.4$, respectively. With these apparent magnitude limits, we compute the number of quasars per square degree per unit redshift from the above-mentioned luminosity functions.

The solid curves in the two panels of Figure 4 show the results of these calculations. Sharp dips at $z \sim 2 - 2.2$ are an artifact of using the Boyle (1991) luminosity function close to the redshift limit of the Boyle et al. (1988) survey. More broadly, the shapes of these curves reflect the interplay between the peak in the quasar luminosity function at $z \sim 2 - 3$ and the smaller fraction of the luminosity function that is visible above the apparent magnitude limit at larger distances. Of course, $F(z)$ is also affected by the increase of the differential volume element dV/dz with z, especially at low redshift. Up to $z \sim 2$, the evolution effects and the magnitude limit work in different directions, producing a relatively flat redshift distribution. Above $z \sim 2$ both the number density of quasars and our ability to see them decreases, and the redshift distribution drops rapidly towards zero.

Since these calculated redshift distributions are only approximate — the quasar luminosity function is itself uncertain, and we have not modeled the selection criteria and corresponding incompleteness of the two surveys in any detail — we fit them with simple analytic forms to use in our Monte Carlo calculations below. These fits are indicated by the dashed curves in Figure 4. The survey's target selection algorithms will probably focus on

objects with point-source morphology in order to reduce contamination by galaxies. This selection technique may exclude quasars at low redshift, where the host galaxies are bright enough to be detected as extended emission. In our $F(z)$ fits, we model this effect by a sharp cutoff at $z < 0.4$.

4.2. Generating Monte Carlo simulations

For our Monte Carlo experiments, we wish to generate realizations of *measured* redshift-space correlation functions $\xi(s, \mu)$ for various cosmological models and quasar survey parameters. We consider two classes of cosmological models: flat models with $\Omega_0 + \lambda_0 = 1$, and open models with $\lambda_0 = 0$. The $\Omega_0 = 1$, Einstein-de Sitter cosmology is a limiting case of both families. We assume that the real-space quasar correlation function is a power-law, $\xi(r) = (r/r_0)^{-\gamma}$, out to $2r_0$. Once the cosmological model, the correlation function parameters, and the quasar survey parameters are set, the expected number of pairs in a separation/redshift bin $ds d\mu dz$ is given by equation (31).

Because the sparseness of the quasar distribution puts us in the Poisson limit (see §3), we are able to generate realizations of the measured $\xi(s, \mu)$ very simply, without creating artificial spatial distributions. Given the expected number of pairs in a bin from equation (31), the number of pairs in a Monte Carlo realization is a random deviate drawn from a Poisson distribution with this mean value. The pair numbers for each bin can be generated independently. In practice we use 20 logarithmic bins in s, starting at $0.1s_0$ and going up to $2s_0$. We use 5 equal bins in μ; because these bins are large, we compute the predicted number of pairs by numerical integration over the bin. We work with redshift bins $\Delta z = 0.15$, implying 12 bins for simulations with a 2dF-like $F(z)$ and 22 bins for simulations with an SDSS-like $F(z)$. We perform simulations for seven cosmological models: flat and open low-density models with $\Omega_0 = 0.1, 0.2, 0.4$, and the Einstein-de

Sitter cosmology, $\Omega_0 = 1$. To fully specify the theoretical model, we must also specify the correlation length s_0 and the index γ as functions of redshift. Existing observations provide only weak constraints on γ. We adopt $\gamma = 2$, close to the index $\gamma = 1.8$ of the galaxy correlation function, and we assume that γ is independent of redshift.

Even the quasar correlation length s_0 is poorly known at present, because the sparseness of the quasar distribution in current samples makes measurements of the quasar correlation function very noisy. The best existing study is probably that of Shanks & Boyle (1994, hereafter SB), who combine data from three quasar redshift surveys. For an $\Omega_0 = 1$, $\lambda_0 = 0$ cosmology, they find that their correlation function measurements are consistent with a quasar correlation length $r_0 = 6\mathrm{h}_0^{-1}$ Mpc that remains constant in comoving coordinates, implying

$$s_0 \equiv \frac{r_0}{g} = 0.002(1+z)^{3/2}, \tag{32}$$

where we use equation (6) for $g(z)$.

In order to scale the SB results to other cosmological models, we note that the property of the correlation function most robustly constrained by observations is the total number of correlated pairs. From equation (20), we see that the number of correlated pairs is

$$N_{pairs}(z) \propto \frac{r_0^3}{\tilde{g}\tilde{f}^2} \propto \frac{s_0^3 g^2}{f^2} \propto \frac{s_0^3}{h^2}, \tag{33}$$

where we have dropped the factors that are independent of the spacetime geometry. For alternative cosmological models, we therefore wish to hold the combination s_0^3/h^2 equal to the value implied for the $\Omega_0 = 1$, $\lambda_0 = 0$, $r_0 = 6\mathrm{h}_0^{-1}$ Mpc model that fits the SB data. We therefore adopt

$$s_0(z, \Omega_0\ , \lambda_0) = 0.002(1+z)^{\frac{3}{2}} \left[\frac{h(z, \Omega_0\ , \lambda_0)}{h(z, \Omega = 1, \lambda_0 = 0)} \right]^{\frac{2}{3}} \tag{34}$$

as a fiducial redshift-space correlation length for our simulations.

4.3. Maximum likelihood determination of parameters

Given a simulated or observed set of correlation measurements, we are interested in estimating the true correlation function parameters and the parameters of the underlying cosmological model. Suppose that the data consist of pair counts N_i in i bins, where i may in fact represent a multidimensional (e.g. s, μ) space. We have a model $\mathcal{M}$ for the correlation function that may depend upon several parameters, e.g. $\mathcal{M}(s_0, \gamma, \Omega_0\ , \lambda_0\)$. This model predicts a number of pairs in each bin $A_i = \bar{n} V_i (1 + \xi(s_i, \mu_i)) N_Q$, where V_i is the bin volume. In the Poisson limit $N_c \lesssim 1$, which is expected to hold for realistic quasar surveys (see §3), the probability of detecting N_i pairs in bin i when A_i are expected is

$$P(N_i|A_i) = \frac{e^{-A_i} \cdot A_i^{N_i}}{N_i!}. \tag{35}$$

The probabilities for separate bins are independent, so the overall likelihood $\mathcal{L}$ of obtaining the data given the model is

$$\mathcal{L} \equiv P(D|\mathcal{M}) = \prod\nolimits_i \frac{e^{-A_i} \cdot A_i^{N_i}}{N_i!}, \tag{36}$$

implying

$$\ln(\mathcal{L}) = \sum\nolimits_i (-A_i + N_i \ln\ A_i - \ln\ N_i!). \tag{37}$$

Since the data N_i are independent of the model parameters, one can find the maximum likelihood model by maximizing the quantity

$$\ln \mathcal{L}^{'}(\mathcal{M}) = \sum_i (N_i \ln\ A_i - A_i). \tag{38}$$

The relative likelihood of two models $\mathcal{M}_1$ and $\mathcal{M}_2$ is simply $\exp(\ln \mathcal{L}'(\mathcal{M}_1) - \ln \mathcal{L}'(\mathcal{M}_2))$.

Although our focus in this paper is on constraining λ_0 , the maximum-likelihood technique outlined here is quite general. For a specified cosmology, one can use this technique to estimate correlation function parameters in a way that makes maximum use of the available data (e.g., Stephens et al. 1997), and the method can easily be extended to incorporate parametrized descriptions of peculiar velocity distortions, evolution of clustering, and so forth. The sparse sampling limit is crucial to this approach, for it is only this property that makes it possible to write down a straightforward expression for the likelihood, equation (36). For a dense sample like a typical galaxy redshift survey, the likelihood is a much more complicated function of the model parameters and the data, and a maximum-likelihood approach is correspondingly more cumbersome. However, rich galaxy clusters do provide a sparse tracer of structure on large scales, and Croft et al. (1997) have used the same maximum-likelihood method to estimate parameters of the cluster correlation function.

4.4. Results

Figures 5–9 present our main results. In Figure 5 we examine the ability of the 2dF (left) and SDSS (right) quasar samples to constrain Ω_0 in flat, $\Omega_0 + \lambda_0 = 1$ models. For each survey and each value of $\Omega_0 = 0.1$, 0.2, 0.4, and 1, we generated four realizations of measured $\xi(s, \mu)$ by the Monte Carlo technique described in §4.2. In all cases we set $\gamma = 2$ and adopt equation (34) for $s_0(z)$, corresponding to $r_0 = 6\mathrm{h_0}^{-1}$ Mpc comoving at all z for the $\Omega_0 = 1$, $\lambda_0 = 0$ model and to $s_0(z = 0) = 0.002$ in all models. For each realization, we then determine the best-fit model parameters by the maximum-likelihood technique described in §4.3, computing likelihoods for a grid of open models and a grid of flat models with $0 \leq \Omega_0 \leq 1$ and varying values of s_0 and γ. Squares show the estimated values of

Ω_0 , denoted $\hat{\Omega}_0$, plotted against the true value Ω_{true} used to generate the realization. Small offsets are added along the Ω_{true} axis to improve clarity. Vertical line segments delineate the range of Ω_0 values that give likelihood values with 10% of the maximum likelihood; this corresponds roughly to a 2σ confidence interval for a Gaussian approximation to the likelihood distribution. In a few cases — mostly $\Omega_0 = 1$ realizations, which are a limiting case of both flat and open models — an open model gave a higher likelihood than the best-fit flat model. For these cases we plot a filled circle at the value of $\hat{\Omega}_0$ for the best-fit open model.

In open cosmologies, the anisotropy of the correlation function is only weakly sensitive to Ω_0 (see Figure 2), so we do not show the analog of Figure 5 for open models. Even with flat models the Ω_0 constraints are rather loose, but it is encouraging to see that in the $\Omega_0 < 1$ models, the $\Omega_0 = 1$ model can be rejected on the basis of quasar clustering anisotropy alone in nearly every case.

There are a number of methods to constrain Ω_0 from the dynamics of redshift-space galaxy clustering (e.g., Kaiser 1987; Carlberg et al. 1996; Kepner, Summers, & Strauss 1997). These methods suffer from a degeneracy between the density parameter and the "bias" of galaxies with respect to mass, but with the high-precision measurements from the 2dF and Sloan *galaxy* redshift surveys it should be possible to break this degeneracy and measure Ω_0 directly. We would then like to use quasar clustering anisotropy to distinguish between open ($\lambda_0 = 0$) and flat ($\lambda_0 = 1 - \Omega_0$) cosmologies of known Ω_0 ; dynamical techniques are insensitive to this distinction because the cosmological constant represents an unclustered energy component.

Figure 6 presents the prospects for such a test. For each realization of each of our low-Ω_0 models, we compute the likelihood ratio $R \equiv \mathcal{L}_2/\mathcal{L}_1$, where $\mathcal{L}_1$ is the likelihood of the true model (with the correct values of Ω_0 , λ_0 , $s_0(z)$, and γ) and $\mathcal{L}_2$ is the likelihood of

the model with the same Ω_0 , $s_0(z)$, and γ but the incorrect geometry. For $\Omega_0 = 0.1$ or 0.2, the incorrect geometry can be rejected at $> 10:1$ odds in all of the 2dF realizations and at $\gtrsim 10:1$ odds in the SDSS realizations. For $\Omega_0 = 0.4$ the difference between geometries is smaller, and the incorrect model can only be rejected at $\sim 10:1$ odds or (occasionally) less. Since the 2dF and SDSS samples will be independent (with telescopes in the southern and northern hemispheres, respectively), a pair of $\sim 10:1$ rejections would constitute a strong statistical result. However, there are uncertainties related to peculiar velocity distortions and evolution of the correlation function that are not incorporated in our current Monte Carlo experiments (see §5 below), so it is not clear that the geometry distinction will be possible with these samples for $\Omega_0 \geq 0.4$.

As equation (20) demonstrates, the precision with which $\xi(s,\mu)$ can be measured depends sensitively on the true quasar correlation length. While the SB estimate is based on the most extensive compilation of existing data, it is nonetheless quite uncertain, and some other studies have suggested higher values. Stephens et al. (1997), for example, find a maximum-likelihood estimate $r_0 = 20\mathrm{h}_0^{-1}$ Mpc (comoving, for $\Omega_0 = 1$, $\Lambda = 0$) for the high-redshift quasars in the Palomar Transit Grism Survey. Figures 7 and 8 repeat the Ω_0 -constraint and geometry-discrimination tests for 2dF (Figure 7) and SDSS (Figure 8) realizations with a correlation length double the value implied by equation (34). This higher correlation length corresponds to $r_0 = 12\mathrm{h}_0{}^{-1}$ Mpc comoving for $\Omega_0 = 1$, $\lambda_0 = 0$, and to $s_0(z=0) = 0.004$ for all models.

With the higher correlation length, incorrect geometry models with $\Omega_0 = 0.4$ are rejected at $\gtrsim 100:1$ odds in all of the 2dF realizations and all but one of the SDSS realizations. With $\Omega_0 \leq 0.2$, the incorrect geometry models are rejected with formal odds exceeding $10^6:1$ in all realizations of both surveys. The Ω_0 determinations in flat models are much more precise than those shown in Figure 5 for the smaller correlation length. It

is of course possible that the true quasar correlation length is *lower* than the SB estimate instead of higher, in which case the prospects for the clustering anisotropy method would be worse than those implied by Figures 5 and 6. The uncertainty in the amplitude of quasar clustering is presently the main uncertainty in assessing the power of future quasar surveys to constrain cosmological parameters by this approach.

Figures 5–8 show that the 2dF survey has somewhat greater constraining power than the SDSS, even though it has 30,000 quasars instead of 80,000. The high surface density of the 2dF sample is crucial to its performance; the factor N_Q^2/A in equation (20) for the number of correlated pairs is nearly the same for the 2dF and the SDSS. The reason the 2dF survey does slightly better is its more compact redshift distribution $F(z)$. The SDSS has roughly equal numbers of quasars per unit redshift from $z = 0.4$ to $z = 2.2$, and a significant fraction of the sample lies at $z > 2.2$. For the 2dF survey, a majority of the quasars lie in the range $1 < z < 2.2$. The number of correlated pairs per unit redshift is proportional to $[F(z)]^2$, and the more precise measurement of $\xi(s, \mu)$ at $z \sim 2$ in the 2dF sample wins out over the greater range of redshifts probed by the SDSS.

As this comparison suggests, the ability of a quasar survey to measure clustering anisotropy is sensitive to its details, and there are strategies that can substantially enhance this ability for a fixed number of quasars. One possible approach would be to use multi-color selection techniques to target quasars in particular redshift ranges, producing peaks in $F(z)$ at specific redshifts. Another approach is simply to observe a smaller area to a fainter magnitude limit, thus increasing N_Q^2/A. Either strategy improves the survey's sensitivity to geometrical distortion (at the cost of longer spectroscopic exposures), provided that the clustering measurements remain in the sparsely sampled regime, $N_c \lesssim 1$. Once N_c exceeds one, new quasar pairs contribute partially redundant information, and there is more to be gained by expanding the survey's area or redshift range. (This statement applies only to

the two-point correlation function and its relatives; clustering measures that are sensitive to higher-order correlations would continue to benefit from denser sampling.)

As an illustration, we repeat the tests of Figures 5–8 for a hypothetical high density quasar survey (HDS), now returning to the smaller quasar correlation length implied by equation (34). We assume a sample of 30,000 quasars in 200 square degrees — the same N_Q as 2dF, but a surface density 3.25 times higher, and $F(z)$ identical to the one of 2dF. The Sloan southern stripe quasar survey might provide such a sample if quasars can be identified and their redshifts measured to a sufficiently faint limiting magnitude. Figure 9 shows that even with the small correlation length, the high-density survey allows strong rejection of models with incorrect geometry in all realizations with $\Omega_0 = 0.1$ or 0.2 and in most realizations with $\Omega_0 = 0.4$.

Although we have focused mainly on the sensitivity of planned surveys to Ω_0 and λ_0, we should note that in our experiments the 2dF and SDSS samples constrain γ and s_0 to at least 10% accuracy, with typical accuracy of about 5%. In the cases with a high quasar correlation length or a high-density quasar survey, the maximum-likelihood estimates achieve 2–3% accuracy in recovering γ and 1–3% accuracy in recovering s_0. We can thus expect these future surveys to provide precise measurements of the basic parameters characterizing the quasar correlation function.

5. Discussion

Our results from §4.4 show that the ambitious quasar redshift surveys planned by the 2dF and SDSS teams can make important contributions to the study of the geometry of spacetime. In the case of flat cosmological models, some constraints on Ω_0 can be obtained even for the SB correlation length, and these constraints become interestingly tight for a

high-density quasar survey or for the 2dF and SDSS if the correlation length is a factor of two larger than SB's estimate. Clustering anisotropy does not provide useful constraints on Ω_0 in open models because the distortion parameter $h(z)$ is insensitive to Ω_0 , and there is a near degeneracy in $h(z)$ between an open model with low Ω_0 and a flat model with a higher Ω_0 . The true power of the clustering anisotropy technique comes into play if Ω_0 itself is determined independently by dynamical methods. Clustering anisotropy then provides a tool for discriminating between open models with $\lambda_0 = 0$ and flat models with $\lambda_0 = 1 - \Omega_0$, a distinction that is difficult to achieve with dynamical methods alone. We find that clear discrimination between flat and open geometries is possible for the 2dF and SDSS samples with the SB correlation length if $\Omega_0 \leq 0.2$, but the discrimination is only marginal for $\Omega_0 = 0.4$. The high-density survey with the SB correlation length or the 2dF or SDSS for double the SB correlation length provide clear discrimination for $\Omega_0 = 0.4$.

The results in Figures 5–9 look fairly promising, but there are some limitations in our numerical experiments. For example, we assumed no evolution in γ and a fixed form of $s_0(z)$ (corresponding to no comoving evolution for $\Omega_0 = 1$, $\Lambda = 0$), so that we could produce one global fit to the clustering and cosmological parameters using all of the data. In the real universe, one will have to allow for the possibility of different evolution of the correlation function parameters. The maximum-likelihood method described in §4.3 adapts easily to this if the evolution can be described in a parametrized form, but because there can be some tradeoff between different effects, adding new parameters will weaken the constraints on Ω_0 and λ_0. Also, as we have already noted, our assumed values of s_0 and γ, while plausible, are highly uncertain. If s_0 and γ turn out to be larger than we have assumed, then the statistical power of the clustering anisotropy test will increase; if smaller it will decrease.

Probably the most important element missing in our analysis is the effect of peculiar

velocities, since small scale velocity dispersions and large scale coherent flows can both induce an angular dependence in $\xi(s,\mu)$. To a first approximation, the small-scale dispersion has the effect of convolving the correlation function along the line of sight with the pairwise velocity distribution function (Davis & Peebles 1983; see also Fisher 1995). This causes a large distortion of the correlation function for galaxies at $z = 0$. However, if $s_0 = 0.01$ at $z = 2$, then the velocity scale corresponding to the correlation length is $0.01c = 3000\,\mathrm{kms}^{-1}$. The dispersion velocity of quasars is unknown, but a plausible value is $\sim 300\,\mathrm{kms}^{-1}$ — the velocity dispersion of typical galaxy group. The width of the distribution function is thus very small compared to the correlation length, so for pairs separated by $\sim s_0$, the distortion due to small scale dispersion should be small.

Coherent large scale motions pose a potentially more serious problem. As a rough gauge of the importance of those velocities in confusing geometrical distortion, we can estimate the ratio of $\xi(s,1)/\xi(s,0)$ resulting from geometry and from linear theory peculiar velocities. For the surveys that we have considered, most of the geometrical information comes from the redshift $z \sim 2$, so we will take this value as the fiducial one. For typical cosmological models, $h(z) \sim 2$ at $z = 2$, which means that $\xi(s,1)/\xi(s,0) \approx 3.5$ for geometrical distortions alone (see equation [9]). In conventional notation,

$$\beta \approx \frac{\Omega^{0.6}}{b} \tag{39}$$

is the linear theory ratio of peculiar velocity convergence $-\nabla \cdot \mathbf{v}_{pec}/H$ to the galaxy density contrast, where b is the bias parameter relating galaxy and mass fluctuations. If $\beta \ll 1$, then equations (10) and (11) of Hamilton (1992) allow us to write

$$\frac{\xi(s,1)}{\xi(s,0)} = 1 - \frac{2\beta\gamma}{(3-\gamma)+2\beta} \tag{40}$$

We justify equation (40) in appendix A and argue that the typical value of β (assuming the

SB quasar correlation length) is $\sim 1/6$ in open, flat, and Einstein-de Sitter cosmological models. With $\gamma = 1.8$, the ratio (40) then becomes

$$\frac{\xi(s,1)}{\xi(s,0)} \approx 0.6 \tag{41}$$

Thus, the effect of coherent peculiar velocities by no means overwhelms the geometric signal, but it is not negligible. Analyses of real data will have to fit jointly for peculiar velocity distortions and geometrical distortions, using their different angular and redshift dependences to separate them. The results of Ballinger et al. (1996), Matsubara & Suto (1996), and Nakamura et al. (1997) provide important steps towards this goal, though it is not clear whether the linear theory formula for velocity distortions will be adequate near $\xi \sim 1$. A suitably parametrized description of peculiar velocity distortions can easily be incorporated in the maximum-likelihood scheme. The geometrical distortion is weakest in the models with low values of h (low Ω_0 , high λ_0 models). However, these are also the models for which open and flat geometries are most easily distinguished, so there is good reason to believe that such distinctions will remain possible even when the effects of peculiar velocities are taken into account.

There are other routes to measuring or limiting the cosmological constant. Probably the most solid existing limits come from the statistics of gravitational lensing (see, e.g., Carroll, Press, & Turner 1992; Maoz & Rix 1993; Kochanek 1996). These limits are somewhat dependent on assumptions about the evolution of the galaxy population (Rix et al. 1994), but current results present a strong case that $\lambda_0 < 0.8$. A promising approach on the horizon is the application of the classical magnitude-redshift test to calibrated candles in the form of high-redshift, Type Ia supernovae (Perlmutter et al. 1997). This technique is technically challenging, since one must guard carefully against differential selection biases between low- and and high-redshift samples, but if these obstacles can be overcome it is one of the most powerful methods for constraining λ_0 . This approach relies on the plausible

but not incontrovertible assumption that the luminosities of Type Ia supernovae do not change systematically over the age of the universe (see von Hippel, Bothun, & Schommer 1997). High-resolution maps of the cosmic microwave background, such as those expected from the MAP and Planck surveyor satellites, offer another promising route to constraining λ_0 , along with a host of other cosmological parameters (see, e.g., Bennett et al. 1995 and Jungman et al. 1995), at least in the context of cosmic inflation models. It is not yet clear which of these approaches will ultimately yield the best constraints on the cosmological constant, but the existence of four essentially independent methods, all of them able to produce interesting results in the next 5-10 years, is very encouraging. Either they will all yield consistent answers, in which case they provide not just a convincing constraint but a consistency test of the underlying cosmological picture that motivates them, or they will not, in which case they point to a breakdown in the implicit assumptions behind one or more of the methods.

As an extension of this last point, we note that all of our 2dF and SDSS realizations in Figure 5 are inconsistent at the $> 2\sigma$ level with the Euclidean, $\lambda_0 = 1$, $\Omega_0 = 0$ model even for a flat geometry with Ω_0 as low as 0.1 — and the inconsistency is much stronger for higher Ω_0 , a higher quasar correlation length (Figures 7 and 8), or a higher density quasar survey (Figure 9). These results imply that the geometrical distortion described in §2 should be detected by these surveys, even if the discrimination between flat and open space geometries is weak. This distortion is a fundamental property of the cosmological spacetime curvature predicted by General Relativity. If the universe is as we believe it to be, this signature of curved spacetime should be detected within the next decade, and perhaps within the next few years.

We thank Jim Gunn for seminal discussions at the outset of this project. We thank Heidi Newberg, Brian Yanny, Don Schneider, and other members of the SDSS Quasar

Working Group for helpful discussions of plans for the SDSS quasar survey. We thank Tom Shanks for information about the 2dF quasar survey and for helpful discussions on recent estimates of quasar clustering. We acknowledge support from NASA Theory Grant NAG5-3111.

A. The value of the coherent flow parameter β

Hamilton (1992) gives the linear theory distortions of $\xi(s,\mu)$ caused by peculiar velocities:

$$\xi(s,\mu) = \xi_0(r)P_0(\mu) + \xi_2(r)P_2(\mu) + \xi_4(r)P_4(\mu) \tag{A1}$$

where P_i are Legendre polynomials and ξ_0, ξ_2 and ξ_4 are defined in terms of the growth parameter β and the volume-averaged correlation function $\bar{\xi}(r) \propto r^{-\gamma}$ as

$$\xi_0 = -\left(1 + \frac{2\beta}{3} + \frac{\beta^2}{5}\right)\frac{\gamma-3}{3}\bar{\xi}(r) \tag{A2}$$

$$\xi_2 = -\left(\frac{4\beta}{3} + \frac{4\beta^2}{7}\right)\frac{\gamma}{3}\bar{\xi}(r) \tag{A3}$$

$$\xi_4 = \frac{8\beta^2}{35}\frac{\gamma(\gamma+2)}{3(5-\gamma)}\bar{\xi}(r). \tag{A4}$$

Recall that β is defined as

$$\beta = \frac{\Omega^{0.6}}{b}. \tag{A5}$$

For $\beta \ll 1$, only the first two addends in (A1) influence the result, since they contain terms proportional to β but ξ_4 is proportional to β^2. Using the Legendre polynomial definitions $P_0 = 1$ and $P_2 = \frac{3\mu^2-1}{2}$ and neglecting all the terms proportional to β^2, we find

$$\xi(s,1) = \left(1 + \frac{2\beta}{3} - \frac{\gamma}{3} - \frac{2}{3}\beta\gamma\right)\bar{\xi} \tag{A6}$$

$$\xi(s,0) = \left(1 + \frac{2\beta}{3} - \frac{\gamma}{3}\right)\bar{\xi} \tag{A7}$$

Dividing (A6) by (A7) yields

$$\frac{\xi(s,1)}{\xi(s,0)} = 1 - \frac{2\beta\gamma}{(3-\gamma)+2\beta} \tag{A8}$$

equation (40) of the main text.

For $\Omega_0 = 1$, $s_0 = 0.01$ at $z = 2$ corresponds to $6h^{-1}$Mpc comoving, which happens to be roughly the correlation length of bright galaxies today. Observations suggest that these galaxies have $\beta \sim 0.5$, which implies a bias parameter $b = 2$ for $\Omega_0 = 1$. The linear mass fluctuations in an $\Omega_0 = 1$ universe scale with z as $1/(1+z)$, so the implied bias factor for quasars at $z = 2$ is $b \sim 2(1+z) \sim 6$. Thus,

$$\beta(\Omega_0 = 1, \lambda_0 = 0) \sim \frac{1}{6}. \tag{A9}$$

Now consider an open universe with $\Omega_0 \sim 0.3$[3]. The comoving scale gs_0 corresponding to $s_0 = 0.01$ at $z = 2$ is, in this case, larger by a factor of about 1.5 than in the $\Omega_0 = 1$ model. This implies that quasars are clustered more strongly than present-day bright galaxies by a factor of about $1.5^{1.8} \sim 2$. In an open universe, the ratio of the rms present-day mass fluctuation σ_0 to the rms fluctuation $\sigma(z)$ at redshift z is approximately

$$\frac{\sigma_0}{\sigma(z)} = 1 + \frac{2.5\Omega_0}{1+1.5\Omega_0} \cdot z. \tag{A10}$$

The bias parameter of galaxies is $b \sim 1$ at $z = 0$ if $\Omega_0 \sim 0.3$, so the implied bias parameter for quasars at $z = 2$ is

$$b \sim 2 \cdot 1 \cdot \frac{\sigma_0}{\sigma(z)} = 4. \tag{A11}$$

[3]We choose $\Omega_0 = 0.3$ to get some idea about both $\Omega_0 = 0.4$ and $\Omega_0 = 0.2$ cases.

At $z = 2$, the value of the density parameter Ω is

$$\Omega = \frac{(1+z)\Omega_0}{1+\Omega_0\ z} \approx 0.56. \tag{A12}$$

Putting these results together, we get β for quasars at $z = 2$ in a low-density, open universe:

$$\beta(\Omega_0\ = 0.3, \lambda_0 = 0) \sim \frac{0.71}{4} \approx 0.18. \tag{A13}$$

The analysis for a low-density flat universe with $\Omega_0\ \sim 0.3$ follows similar lines. The correlation length is larger by a factor of about 1.8 relative to the $\Omega_0\ = 1$ model. The ratio of mass fluctuations at $z = 2$ to fluctuations at $z = 0$, computed by the appropriate numerical integral, is

$$\frac{\sigma_0}{\sigma(z)} = 2.38. \tag{A14}$$

The implied bias parameter for quasars at $z = 2$ is

$$b \sim 1.8^{1.8} \cdot 2.38 \approx 6.86. \tag{A15}$$

At $z = 2$, the value of Ω is 0.92, and consequently

$$\beta(\Omega_0\ = 0.3, \lambda_0 = 0.7) \sim 0.14. \tag{A16}$$

In all three cases we find

$$\beta(\Omega_0\ , \lambda_0, z = 2) \sim \frac{1}{6}, \tag{A17}$$

so the assumption that $\beta \leq 0.2$ for quasars at $z = 2$ is fairly secure, unless the quasar correlation length is significantly *smaller* than the SB value (in which case detection of geometrical distortions of the correlation function may be rather difficult).

REFERENCES

Alcock, C., Paczyński, B. 1979, Nature, 281, 358

Ballinger, W.E., Peacock, J.A., Heavens, A.F., astro-ph/9605017

Bennett, C.L., Hinshaw, G., Jarosik, N., Mather, J.S., Meyer, S.S., Page, L., Skillman, D., Spergel, D.N., Wilkinson, D.T., Wright, E.L. 1995, BAAS, 187, 7109B

Boyle, B. J. 1991, in Ann. NY Acad. Sci. 647, Texas/ESO-CERN Symposium on Relativistic Astrophysics, Cosmology, and Fundamental Physics, ed. J. D. Barrow, L. Mestel, & P. A. Thomas, 14

Boyle, B. J., Shanks, T., Peterson, B. A. 1988, MNRAS, 235, 935

Carlberg, R. G., Yee, H. K. C., Ellingson, E., Abraham, R., Gravel, P., Morris, S., & Pritchet, C. J. 1996, ApJ, 462, 32

Carroll, S. M., Press, W. H., & Turner, E. L. 1992, ARA&A, 30, 499

Croft, R.A.C., Dalton, G.B., Efstathiou, G., Sutherland, W., Maddox, S., MNRAS, submitted, astro-ph/9701040

Davis, M., Peebles, P.J.E., 1983, ApJ, 267, 465

Fisher, K. B. 1995, ApJ, 448, 494

Hamilton, A.J.S., 1992, ApJ, 385, L5

Jungman, G., Kamionkowski, M., Kosowsky, A., & Spergel, D. N. 1995, Phys Rev D, 54, 1332

Kaiser, N. 1987, MNRAS, 227, 1

Kepner, J., Summers, F., & Strauss, M. 1997, ApJ, in press, astro-ph/9607097

Kochanek, C. 1996, ApJ, 466, 638

Maoz, D., & Rix, H. 1993, ApJ, 416, 425

Matsubara, T., Suto, Y., 1996, ApJ, 470L, 1M

Nakamura, T. T., Matsubara, T., & Suto, Y. 1997, ApJ, submitted, astro-ph/9706034

Peebles, P.J.E. 1980, The Large Scale Structure of the Universe, (Princeton: Princeton University Press)

Perlmutter, S. et al. 1997, ApJ, 483, 565

Phillipps, S. 1994, MNRAS, 269, 1077

Rix, H., Maoz, D., Turner, E.L., & Fukugita, M. 1994, ApJ, 435, 49

Ryden, B.S. 1995a, ApJ, 452, 25R

Ryden, B.S., Melott, A., 1996, ApJ, 470, 160R

Shanks, T., Boyle, B.J., 1994, MNRAS, 271, 763 (SB)

Soneira, R. M., Peebles, P.J.E., 1978, AJ, 83, 845

Stephens, A.W., Schneider, D.P., Schmidt, M., Gunn, J.E., Weinberg, D.H., 1997, AJ, in press

von Hippel, T., Bothun, G. D., & Schommer, R. A., AJ, in press, astro-ph/9706113

Warren, S. J., Hewett, P. C., Osmer, P. S. 1994, ApJ, 421, 412

Weinberg, S. 1972, in "Gravitation and Cosmology" (New York: Wiley)

This manuscript was prepared with the AAS LaTeX macros v4.0.

Fig. 1.— Geometry of an observer and a quasar pair in redshift space, with the distances s, s_θ and s_z indicated.

Fig. 2.— The distortion parameter $h(z)$ as a function of redshift, for the indicated combinations of density parameter Ω_0 and cosmological constant contribution λ_0. A cosmological model with $\Omega_0 = 0$, $\lambda_0 = 1$ would have $h(z) = 1$ at all redshifts.

Fig. 3.— The angular dependence of the correlation function for different values of the distortion parameter h.

Fig. 4.— F(z) for 2dF (left panel) and SDSS (right panel) with superimposed dashed curves that correspond to models used in our simulations.

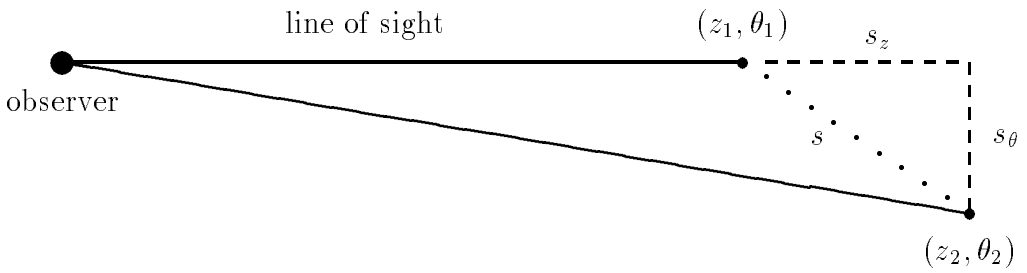
Fig. 5.— Constraints on Ω_0 for flat ($\Omega_0 + \lambda_0 = 1$) cosmological models in simulations of the 2dF (left) and Sloan (right) quasar samples. Eight realizations (four for each survey) were generated for each value of $\Omega_0 = 0.1$, 0.2, 0.4, and 1. In all cases the true correlation function was characterized by $\gamma = 2$, $s_0(z = 0) = 0.002$. Open squares show the maximum-likelihood estimates of Ω_0 ; error bars delineate the range of models with likelihood greater than 10% of the maximum likelihood. Filled circles are plotted in cases where an open model had a higher likelihood than the best-fit flat model. Small horizontal offsets are introduced for clarity.

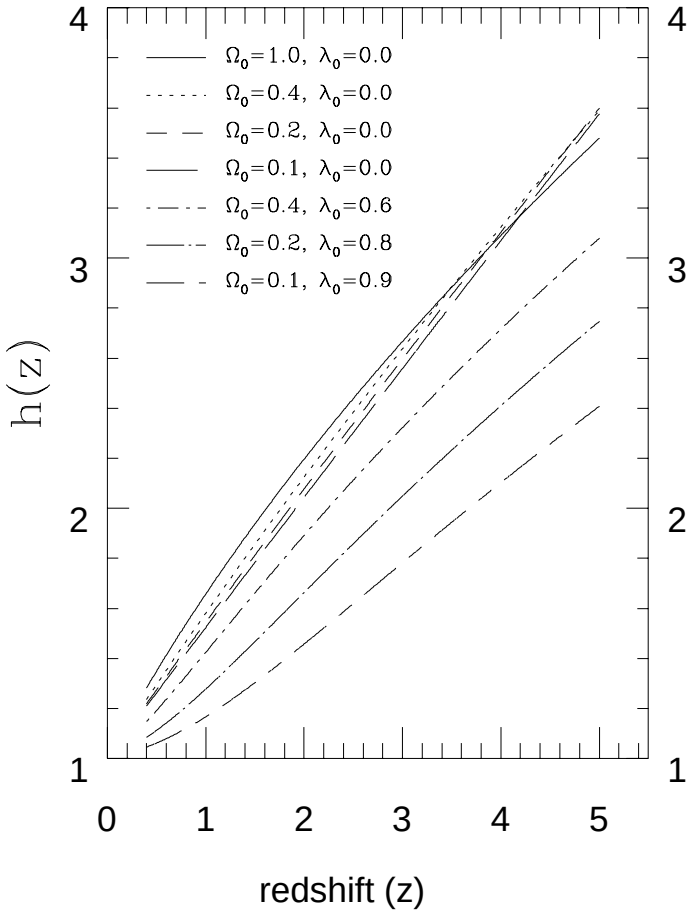
Fig. 6.— Relative likelihoods of flat and open models for simulations of the 2dF (left) and Sloan (right) quasar samples. Triangles represent flat models; R^{-1} is the ratio of the likelihood of the true (flat geometry) model to the likelihood of an open model with the same value of Ω_0 and correlation function parameters. Circles show the corresponding comparison for intrinsically open models. For $\Omega_0 = 0.1$ or 0.2, the incorrect geometry models can usually be rejected with 10:1 confidence or better. Small horizontal offsets have been introduced for clarity.

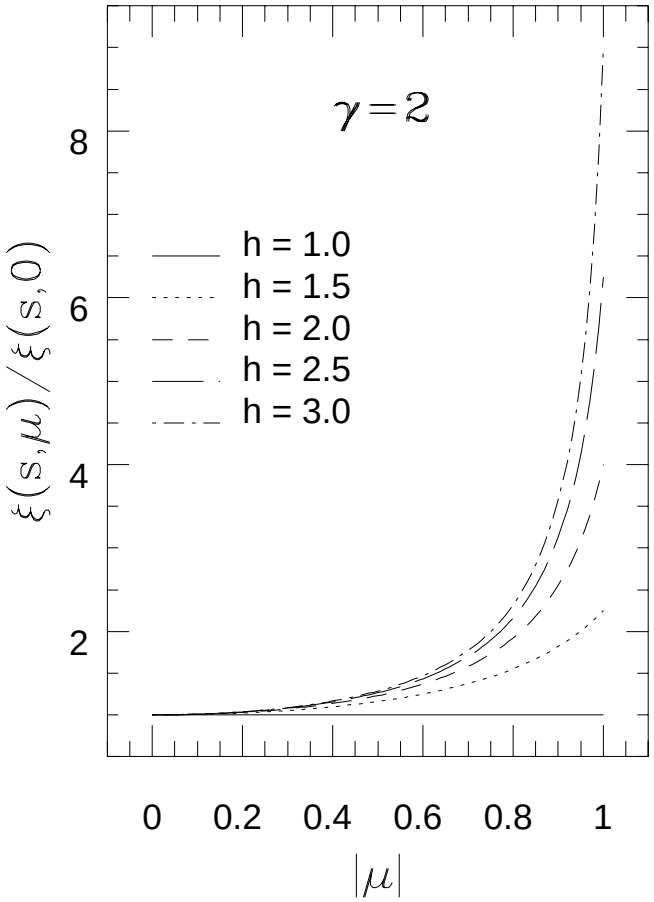
Fig. 7.— Constraints from simulations of the 2dF quasar sample for a high quasar correlation length, $s_0(z = 0) = 0.004$ ($r_0(z = 0) = 12\mathrm{h}_0^{-1}$ Mpc). Left panel shows the ratio of the likelihood of a model with incorrect geometry to the true model, in the same format as Figure 6. Right panel shows constraints on Ω_0 for flat models, in the same format as Fig. 5.

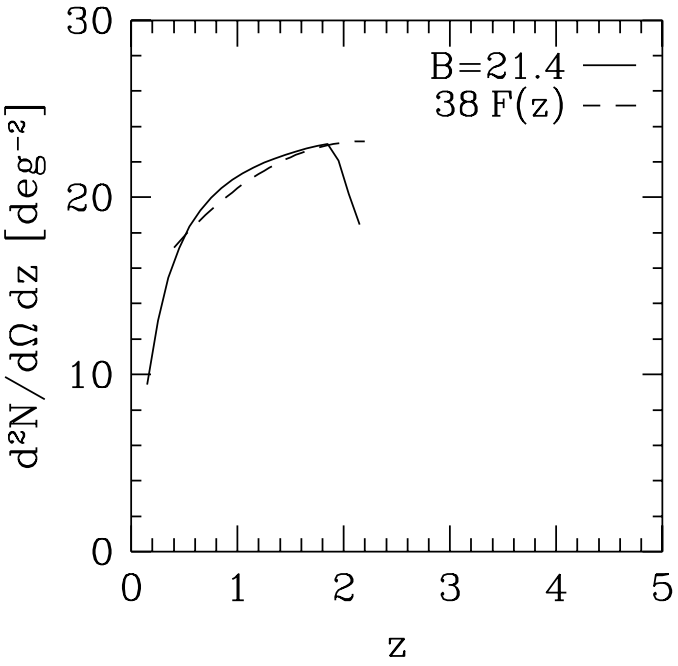
Fig. 8.— Same as Fig. 7, but for simulations of the Sloan sample.

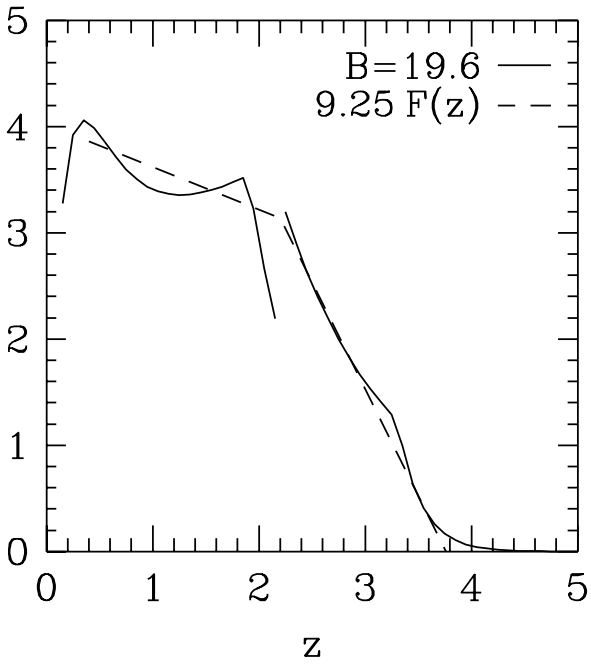
Fig. 9.— Same as Figs. 7 and 8, but for $s_0(z = 0) = 0.002$ ($r_0(z = 0) = 6\mathrm{h}_0^{-1}$ Mpc) and sample parameters of a hypothetical high-surface-density quasar survey, with 30,000 quasars in 200 square degrees.

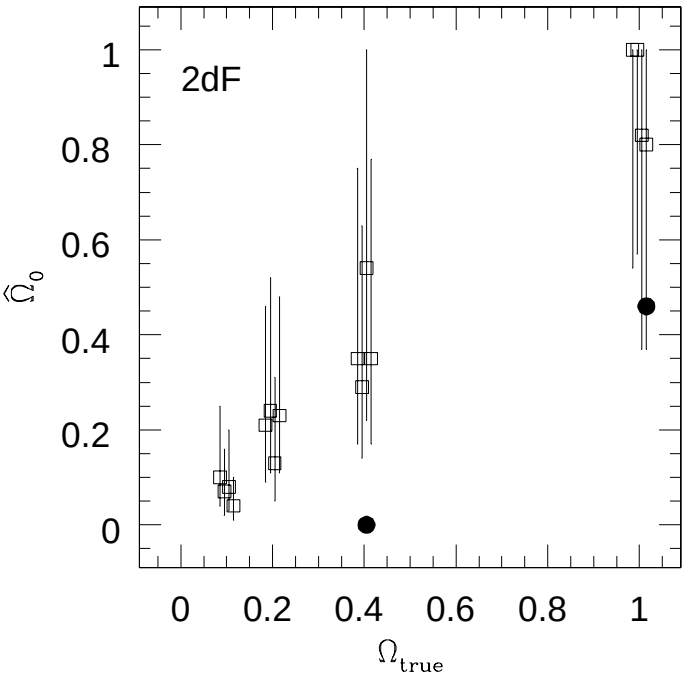

line of sight
(z_1, θ_1)
s_z
observer
s
s_θ
(z_2, θ_2)

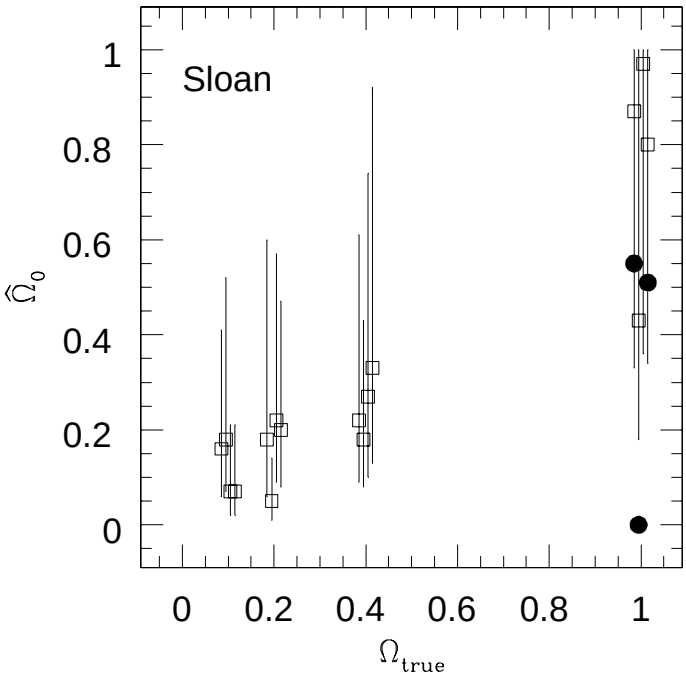

Ω_0=1.0, λ_0=0.0
Ω_0=0.4, λ_0=0.0
Ω_0=0.2, λ_0=0.0
Ω_0=0.1, λ_0=0.0
Ω_0=0.4, λ_0=0.6
Ω_0=0.2, λ_0=0.8
Ω_0=0.1, λ_0=0.9
h(z)
redshift (z)
0
1
2
3
4
5

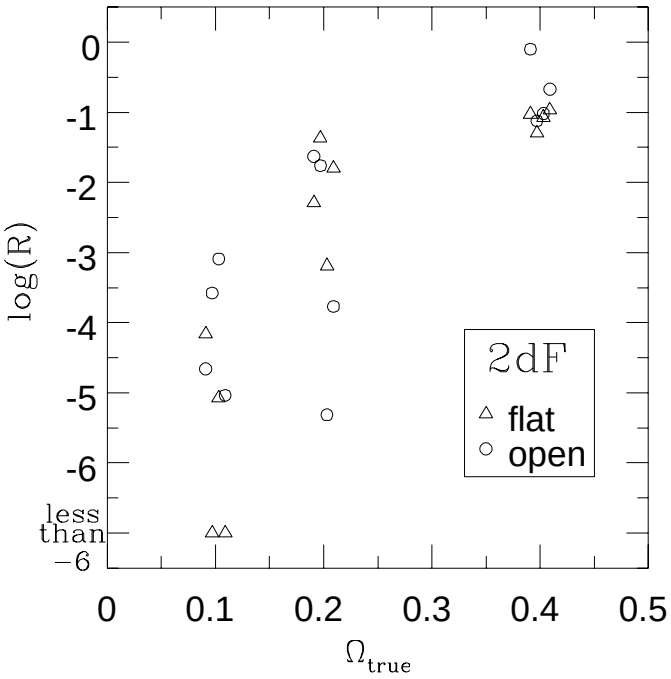

$\gamma = 2$
h = 1.0
h = 1.5
h = 2.0
h = 2.5
h = 3.0
$\xi(s,\mu)/\xi(s,0)$
8
6
4
2
0
0.2
0.4
0.6
0.8
1
$|\mu|$

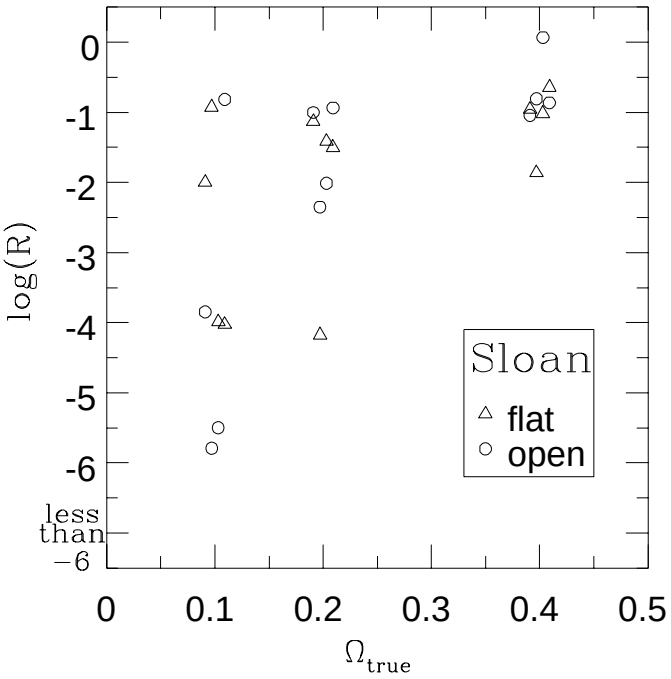

B=21.4
38 F(z)
$d^2N/d\Omega\, dz$ [deg^{-2}]
z

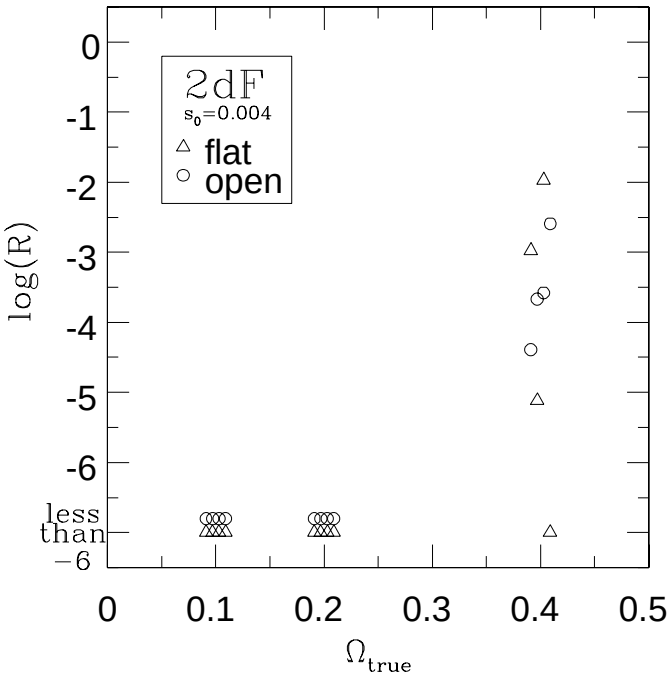

B=19.6
9.25 F(z)
z

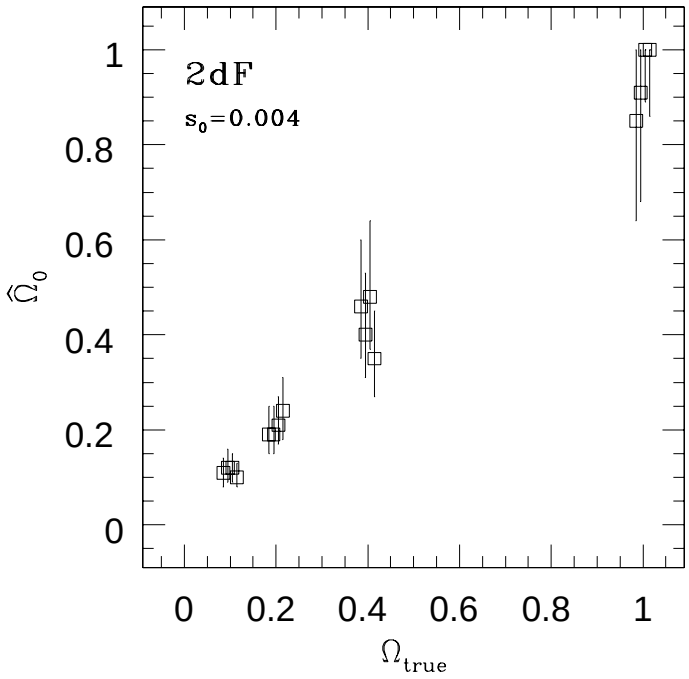

2dF
1
0.8
0.6
0.4
0.2
0
$\hat{\Omega}_o$
0
0.2
0.4
0.6
0.8
1
Ω_{true}

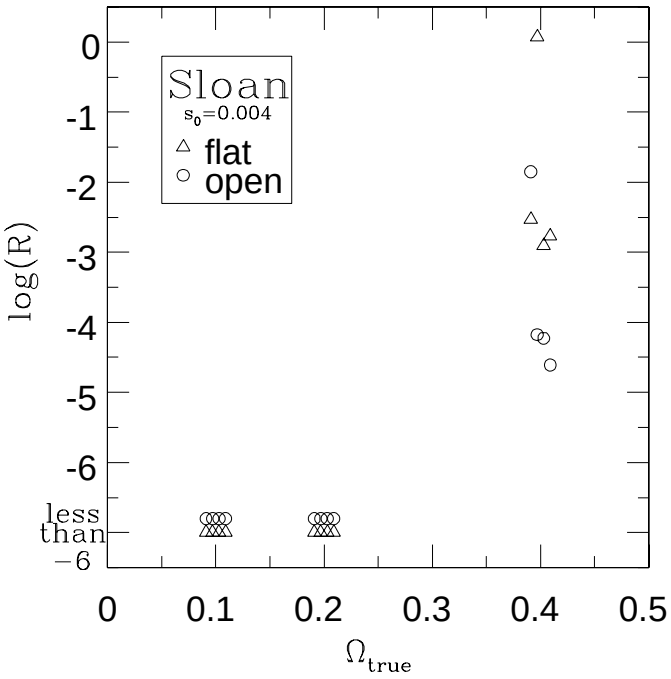

Sloan
1
0.8
0.6
0.4
0.2
0
$\hat{\Omega}_o$
0
0.2
0.4
0.6
0.8
1
Ω_{true}

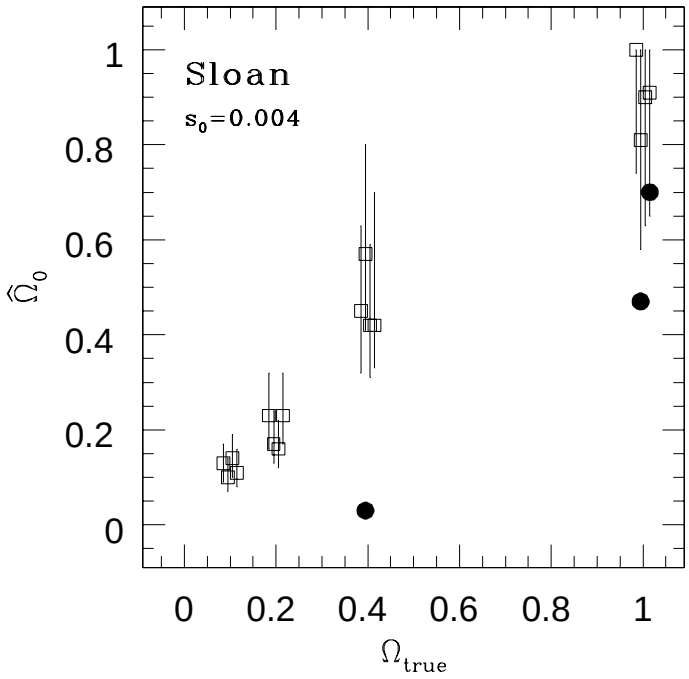

0
-1
-2
-3
-4
-5
-6
less
than
−6
log(R)
0
0.1
0.2
0.3
0.4
0.5
Ω_{true}
2dF
flat
open

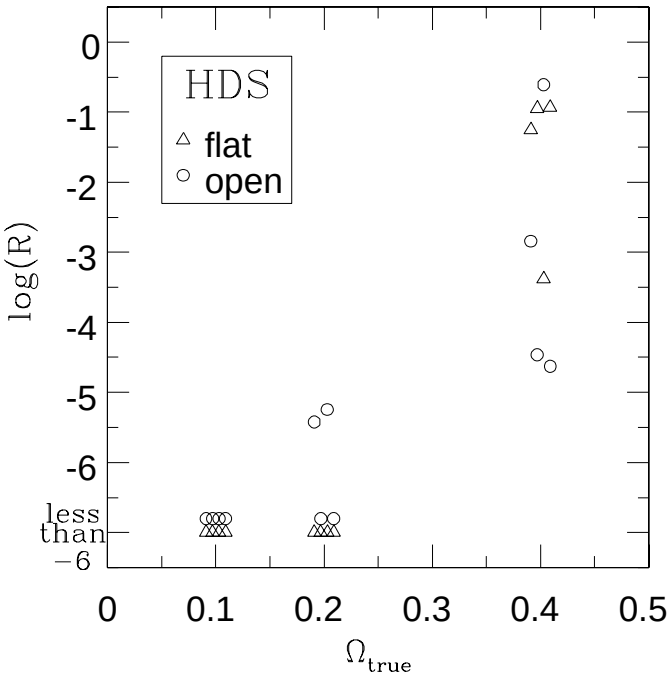

0
-1
-2
-3
-4
-5
-6
less
than
−6
log(R)
0
0.1
0.2
0.3
0.4
0.5
Ω_{true}
Sloan
flat
open

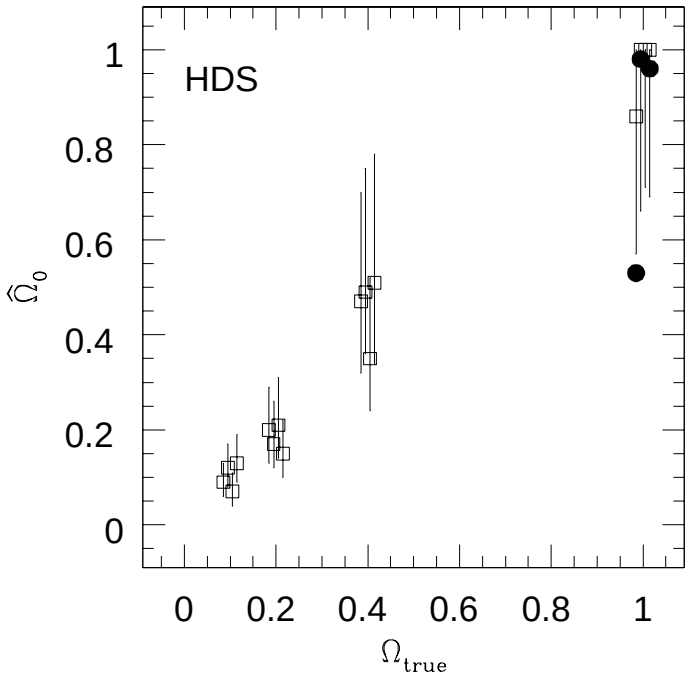

2dF
s_0=0.004
flat
open
log(R)
0
-1
-2
-3
-4
-5
-6
less
than
−6
0
0.1
0.2
0.3
0.4
0.5
Ω_{true}


2dF
s_0=0.004
$\hat{\Omega}_0$
1
0.8
0.6
0.4
0.2
0
0
0.2
0.4
0.6
0.8
1
Ω_{true}


Sloan
s_0=0.004
flat
open
log(R)
0
-1
-2
-3
-4
-5
-6
less
than
−6
0
0.1
0.2
0.3
0.4
0.5
Ω_{true}


Sloan
s_0=0.004
$\hat{\Omega}_0$
1
0.8
0.6
0.4
0.2
0
0
0.2
0.4
0.6
0.8
1
Ω_{true}


HDS
flat
open
log(R)
0
-1
-2
-3
-4
-5
-6
less
than
−6
0
0.1
0.2
0.3
0.4
0.5
Ω_{true}


HDS
$\hat{\Omega}_0$
1
0.8
0.6
0.4
0.2
0
0
0.2
0.4
0.6
0.8
1
Ω_{true}